Plant Biotechnology Journal

WILEY

RESEARCH ARTICLE OPEN ACCESS

UV-B Responsive Flavonoid Synthesis Contributes to Tartary Buckwheat High-Altitude Adaption

Yuanfen Gao[1,2] | Tanzim Jahan[1] | Lin Hao[1] | Yaliang Shi[1] | Chongzhong Ma[1] | Md. Nurul Huda[1] | Hui Chen[2] | Wei Li[1] | Alisdair R. Fernie[3] | Yuqi He[1] | Kaixuan Zhang[1] | Meiliang Zhou[1]

[1]State Key Laboratory of Crop Gene Resources and Breeding, Institute of Crop Sciences, Chinese Academy of Agricultural Sciences, National Crop Gene Bank Building, Beijing, Haidian Region, China | [2]College of Life Sciences, Sichuan Agricultural University, Ya'an, China | [3]Department of Molecular Physiology, Max Planck Institute of Molecular Plant Physiology, Potsdam, Germany

Correspondence: Kaixuan Zhang (zhangkaixuan@caas.cn) | Meiliang Zhou (zhoumeiliang@caas.cn)

Received: 18 May 2025 | **Revised:** 1 July 2025 | **Accepted:** 7 July 2025

Funding: This work was supported by the National Natural Science Foundation of China (32241038).

Keywords: buckwheat | flavonoids | isoquercitrin | rutin | UV-B

ABSTRACT

High-altitude environments expose plants to increased levels of UV-B radiation, necessitating the evolution of protective mechanisms to mitigate stress. Buckwheat is a flavonoid-rich pseudocereal naturally adapted to high-altitude environments with elevated UV-B exposure. Although flavonoid biosynthesis is thought to contribute to this adaptation, the molecular and metabolic basis underlying flavonoid-mediated UV-B tolerance remains largely uncharacterized. In this study, we comprehensively assessed the relationship between flavonoid content and UV-B resistance across several cultivated and wild buckwheat species, including *Fagopyrum esculentum*, *F. tataricum*, *F. cymosum*, *F. gracilipes* and *F. urophyllum*. Our findings demonstrate that the synthesis of rutin strongly correlates with enhanced UV-B tolerance in buckwheat species, and the synthesis of rutin, along with isoquercitrin, positively influences the growth of diverse crops under UV-B stress. Functional validation of key enzymes revealed that the G125D variation in FtFLS4 and variations within the PGSG-box of FtRT1 significantly impact rutin-related metabolite synthesis in buckwheat. Notably, the Tartary buckwheat genes *FtFLS4*, *FtUF3GT1* and *FtRT1* exhibited both catalytic activity and UV-B inducible promoter responses, collectively underpinning *F. tataricum*'s superior UV-B tolerance. Furthermore, we characterised the distinct UV-B response characteristics of *FgFLS4* and *FgFLS7* in the tetraploid wild buckwheat *F. gracilipes*, suggesting diversified adaptive strategies. Our findings provide novel insights into the functional basis of UV-B adaptation in Tartary buckwheat and offer potential targets for breeding or engineering UV-B-resilient crops.

1 | Introduction

Buckwheat (*Fagopyrum* spp.), a pseudograin crop cultivated in the Himalayan region, exhibits remarkable adaptation to high-altitude environments (Zhang et al. 2017). The genus *Fagopyrum* encompasses 21 species, which are morphologically classified into the *cymosum* group (*F. esculentum*, *F. cymosum* and *F. tataricum*) and the *urophyllum* group (*F. gracilipes* and *F. urophyllum*) (Wen et al. 2021). While the distribution ranges of these species vary (Wen et al. 2021), Tartary buckwheat stands out with its ability to thrive at altitudes up to 4500 m, exceeding the typical limit of 3600 m for other species. However, the precise mechanisms underlying this differential high-altitude adaptation remain to be fully elucidated.

High-altitude environments are characterised by reduced air pressure, lower temperatures and intensified ultraviolet-B (UV-B) radiation (Körner 2007). UV-B radiation (280–315 nm) increases with altitude (Häder and Cabrol 2020; Zhang et al. 2016) and poses a significant challenge to plant growth

and development (Kreft et al. 2022; Takahashi et al. 2011). To cope with this stress, high-altitude adapted plants have evolved various strategies (Chen et al. 2022), including Photosystem-II (PSII) and DNA repair mechanisms (Takahashi et al. 2011), and the accumulation of UV-B-absorbing compounds like flavonoids and polyphenols in epidermal cells (Li et al. 2018; Podolec and Ulm 2018; Tian et al. 2024). Furthermore, the induction of reactive oxygen species (ROS) scavenging systems, involving antioxidant enzymes and small molecules such as flavonoids, plays a crucial role (Hsieh and Huang 2007; Mittler et al. 2022; Zeng et al. 2020). Among these defences, flavonoids are recognised as key players in plant responses to UV-B stress.

Buckwheat, as a high-altitude adapted crop, is inherently rich in flavonoids (Kreft et al. 2022; Zhong et al. 2022). However, the flavonoid profiles differ significantly among buckwheat species. For instance, Tartary buckwheat exhibits considerably higher levels of rutin, quercetin, kaempferol and vitexin compared to common buckwheat (Li et al. 2022; Li et al. 2019). Some studies suggest that Tartary buckwheat's superior adaptation to high-altitude environments may be linked to its higher flavonoid content (Golob et al. 2022). Nevertheless, more direct evidence is needed to firmly establish the correlation between rich flavonoid content in buckwheat and its high-altitude adaptability across the *Fagopyrum* genus.

Previous researches have demonstrated that increased expression of flavonoid biosynthesis genes enhances UV-B tolerance (Lin et al. 2021; Zhang et al. 2022), while functional defects in these genes lead to reduced flavonoid levels and consequently decreased UV-B resistance (Ryan et al. 2002). This highlights the potential influence of both gene expression levels and enzyme functionality in flavonoid biosynthesis on plant UV-B tolerance. To address the knowledge gap regarding the role of flavonoid biosynthesis in the differential UV-B adaptation of buckwheat species, this study aimed to characterise the UV-B phenotypes of diverse buckwheat species, including the less-studied wild species *F. gracilipes* (Ohsako et al. 2002) and *F. urophyllum* (Nishimoto et al. 2003), and correlate these phenotypes with their metabolite contents, focusing on the rutin biosynthesis pathway. Moreover, we also investigated the mechanisms underlying the variations in rutin synthesis and UV-B tolerance by comparing the promoter activity, enzymatic functions and UV-B responses of flavonol synthase (*FLS*), flavonoid 3-O-glucosyltransferase (*UF3GT*) and rhamnosyltransferase (*RT*) genes across different buckwheat varieties. Our findings provide novel insights into how flavonoids contribute to plant adaptability to UV-B radiation in the context of high-altitude environments.

2 | Results

2.1 | Flavonoids Contribute to UV-B Tolerance

Buckwheat's well-documented richness in flavonoids contributes to its nutritional value and resilience to environmental stresses such as UV-B, drought, and cold, enabling its cultivation in marginal environments (Kreft et al. 2022; Zargar et al. 2024). While different buckwheat species exhibit variations in flavonoid content, common buckwheat generally has lower levels of quercetin, kaempferol and rutin compared to Tartary buckwheat (Zhang et al. 2023). However, it remains unclear whether these differences affect UV-B adaptability.

To investigate the metabolite profiles of different buckwheat species, we employed a fast LC-QqQ-MS/MS approach (Lai et al. 2025) to quantify 45 metabolites, including proanthocyanidins, coumarins, anthocyanins and flavonoids in the seeds of *F. tataricum* (cv. Pinku and cv. Miqiao), *F. esculentum*, *F. cymosum*, *F. urophyllum* and *F. gracilipes* (Table S1, Figure S1). These species displayed distinct metabolite signatures. For example, *F. tataricum* cultivars Pinku and Miqiao showed high metabolic similarity (Figure S1). Notably, *F. cymosum* and *F. tataricum* exhibited elevated levels of rutin, nicotiflorin, quercetin, kaempferol, afzelin and total flavonoids, while *F. urophyllum* was especially enriched in procyanidin and isoquercitrin (Figure S1).

UV-B tolerance of these buckwheat species was then assessed during seed germination and early seedling growth. Due to the protective role of the endosperm during germination (Yan et al. 2014), we subjected the seeds to UV-B treatment. *F. tataricum* and *F. urophyllum* showed minimal inhibition of seedling elongation under UV-B exposure (Figures 1a and S2). To explore the biochemical basis of this variation, Pearson correlation analysis was performed between metabolite levels and UV-B-induced growth responses. Rutin, nicotiflorin, quercetin, kaempferol, isoquercitrin, cinnamic acid and total flavonoids were positively correlated with seedling growth under UV-B, with isoquercitrin and cinnamic acid showing the strongest association with relative elongation rate (Figure 1b,c).

To further elucidate the role of these metabolites, we utilised *F. esculentum*, known for its accessibility and sensitivity to UV-B, and applied individual flavonoids exogenously. Rutin, quercetin, isoquercitrin, kaempferol and procyanidin significantly promoted seedling growth under UV-B treatment compared to control (Figure 1d,e), supporting their roles in enhancing UV-B tolerance. These findings suggest that the superior UV-B tolerance of *F. tataricum* and *F. urophyllum* is linked to their elevated content of metabolites within the rutin biosynthesis pathway.

To assess the ecological relevance of flavonoid accumulation, we analysed previous data on the elevation distribution of *F. tataricum* germplasms (Lai et al. 2024) alongside published metabolomics datasets (Zhao et al. 2023). Tartary Buckwheat germplasms from elevations above 2000 m had significantly higher levels of rutin, isoquercitrin, taxifolin and aromadendrin than those from lower elevations (Figure S3), suggesting that flavonoid biosynthesis responds to elevation, likely due to increased UV-B exposure at higher altitudes.

Furthermore, to determine whether these UV-B-protective compounds function similarly in other crops, we treated dicotyledons

(cabbage, soybean and mung bean) and staple cereal crops (rice, wheat and barley) with isoquercitrin and rutin under UV-B conditions. Both compounds promoted seedling growth in all six species (Figures 1e,f and S4), indicating that downstream metabolites of the rutin synthesis pathway play a conserved role in enhancing UV-B tolerance across plant taxa.

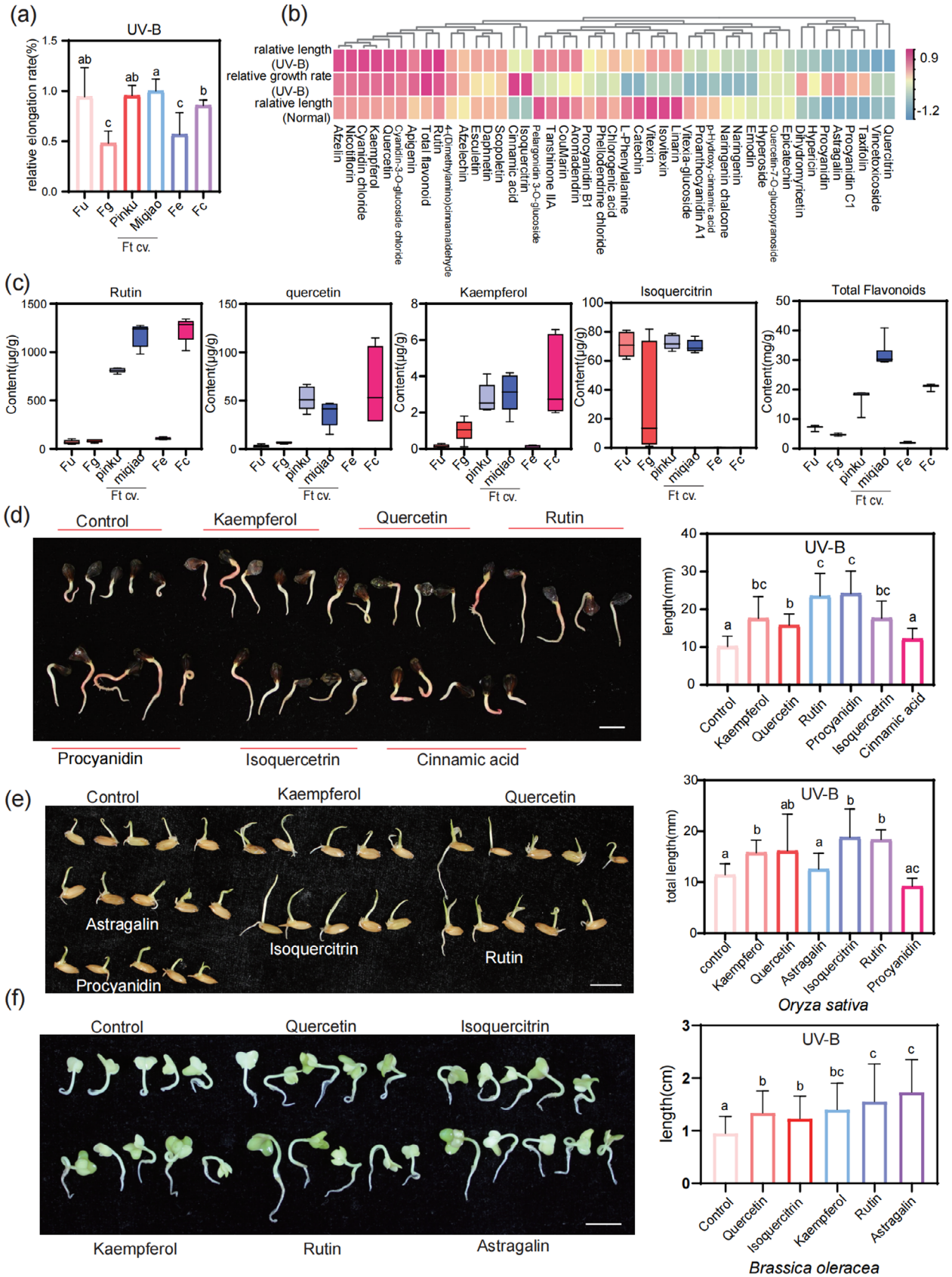

FIGURE 1 | Legend on next page.

FIGURE 1 | Analysis of the relationship between flavonoid content and UV-B tolerance across different buckwheat varieties. (a) Seedling relative growth rates after UV-B treatment. The seedlings were grown for 6 days. The values are means ± SD ($n = 3$ biological replicates). (b) Correlation analysis between the growth status of seedlings under UV-B treatment or normal conditions and the flavonoid content in different buckwheat varieties. The relative length under UV-B is calculated using the length of *F. tataricum* cv. Miqiao under UV-B irradiation as the reference. The relative growth rate under UV-B is calculated using the growth rate of *F. tataricum* cv. Miqiao under UV-B irradiation (compared to the normal condition) as the reference. The relative length under normal conditions is calculated using the length of *F. tataricum* cv. Miqiao as the reference. (c) Flavonoid content in different buckwheat varieties. Kaempferol, quercetin, rutin, isoquercitrin and total flavonoid content in buckwheat. (d) Effects of exogenous flavonoids on the growth of *F. esculentum* seedlings under UV-B stress (left), seedling lengths (right). (e) UV-B treatment of *Oryza sativa*. Kaempferol, quercetin, isoquercitrin, astragalin, rutin and procyanidin were used for treatment (left), with total length measured (right). (f) UV-B treatment of *Brassica oleracea*. Kaempferol, quercetin, isoquercitrin, astragalin and rutin were used for treatment (left), with root length measured (right). The values are means ± SD. One-way ANOVA and Tukey's post-test were used for significance analysis among different groups. Different letters indicate significant differences ($p < 0.05$), while the same letters denote no significant differences.

2.2 | *FtFLS4* and Its Homologues Are Critical for Quercetin Synthesis and UV-B Adaptation in Buckwheat

To understand the genetic basis underlying differences in rutin-related metabolite content among *F. tataricum*, *F. esculentum*, *F. cymosum*, *F. urophyllum* and *F. gracilipes*, we focused on key enzymes involved in the rutin biosynthesis pathway. Flavonol synthase (*FLS*) is a central enzyme responsible for the synthesis of quercetin, a precursor of rutin. Using > 30-fold resequencing data from 200 *F. tataricum* core accessions (Lai et al. 2024) and metabolite GWAS data (Zhao et al. 2023), we identified candidate genes, *FtFLS3 and FtFLS4*, located near a significant SNP associated with quercetin-7-O-(6″-O-malonyl)-β-D-glucoside levels (Figure 2a, Tables S2 and S3).

Analysis of the *FLS* gene family in buckwheat revealed that *FtFLS3* and *FtFLS4* are conserved as tandem repeats in the buckwheat genome, with clear evidence of segmental duplication (Figures S5–S7). This duplication event likely set the stage for their subsequent functional diversification. Indeed, *FtFLS3* was found to be highly expressed in roots, while *FtFLS4* exhibited elevated expression in seeds (Figure S7b). This divergent expression pattern may reflect functional diversification following the gene duplication event (Bright et al. 2017). Although *FtFLS3* (Figure S8a) shares functional similarity with *FtFLS4* (Li et al. 2012), the expression levels of *FtFLS4* and its homologues were more stable compared to *FtFLS3* and its homologues (Figure S7d). Furthermore, selection pressure analysis indicated that the clade containing *FtFLS4* and its homologues underwent positive selection (Figure S7f). These findings collectively suggest that *FtFLS4* and its homologues are likely to play a more pivotal functional role in seed development, whereas *FtFLS3* may have specialised functions primarily in roots.

Phylogenetic analysis divided FtFLS4 homologues into two clusters corresponding to the *cymosum* and *urophyllum* groups, with a protein sequence similarity of 89% (Figure 2b). Notably, FgFLS4 from the *urophyllum* group also demonstrated the ability to catalyse the formation of both quercetin and kaempferol (Figures 2c and S8b). Promoter activity assays showed that *FgFLS4* exhibited the highest promoter activity, while *FtFLS4* and its other homologues displayed relatively similar and stable activity levels (Figure 2d), suggesting a conserved regulatory mechanism for basal expression in buckwheat (Danino et al. 2015). To understand the functional divergence between FLS proteins from the *cymosum* and *urophyllum* groups, the enzyme function of FtFLS4 and FgFLS4 was compared. While both enzymes exhibited similar Km values, FtFLS4 displayed greater catalytic activity (Vmax) and 15% higher activity than FgFLS4 (Figure 2e,f).

To investigate the molecular basis for this activity difference, we conducted molecular docking and site-directed mutagenesis. Molecular docking and site-directed mutagenesis identified two key amino acid residues, located in the predicted catalytic center, which correspond to the Y23F and G125D variations between *FtFLS4* and *FgFLS4* (Figures 2g,h and S8c,d). The *FtFLS4* G125D mutant showed a significant reduction in the formation of both quercetin and kaempferol (Figure 2i,j), and overexpression of this mutant in hairy roots resulted in decreased quercetin and total flavonoid content compared to wild-type *FtFLS4* overexpression (Figure S8e,f). Conversely, the reciprocal D125G mutation in *FgFLS4* led to only a 12% increase in enzyme activity (Figure 2k).

Protein function is closely related to subcellular localization (Gillani and Pollastri 2024). Subcellular localization analysis showed that although the G125D mutation slightly altered the localization of *FtFLS4*, appearing more cytoskeletal, it did not influence its abundance in the cytoplasm (Figure S8g,h). These results indicate that the G125D variation between FtFLS4 and FgFLS4 is a critical determinant of their differing enzyme activities, where FgFLS4 in the *urophyllum* group exhibits only 85% catalytic capacity compared to FtFLS4, potentially contributing to the lower quercetin and kaempferol levels observed in the *urophyllum* group.

To assess their potential roles in UV-B adaptation, we analysed the promoter activity of *FLS* homologues after UV-B treatment. The promoters of *FtFLS4*, *FgFLS7* and *FdFLS2* showed significant induction by UV-B (Figure S9), suggesting their involvement in the adaptative response of buckwheat to UV-B stress, possibly mediated by UV-B responsive elements within their promoters. Interestingly, while *FgFLS4* (homologous to *FgFLS7* but belonging to a different chromosomal group) displayed strong initial activity, it was not induced by UV-B (Figures 2d and S9). In contrast, *FgFLS7* showed substantial activation under UV-B, which may contribute to the adaptation of *F. gracilipes*, a tetraploid weed, to high-altitude environments with intense UV-B exposure.

2.3 | *FtUF3GT1* Is a Key Gene for Rutin Synthesis in Tartary Buckwheat

The buckwheat genome contains multiple copies of glycosyltransferases (Yang et al. 2024). To identify the key genes involved in rutin synthesis in buckwheat, we analysed mGWAS data from Zhao et al. (2023) and identified that *FtUF3GT1* is significantly associated with the content of kaempferol-3-O-glucoside-7-O-rhamnoside in Tartary buckwheat (Figure 3a). Integrated transcriptomic and metabolomic analyses, employing Weighted Gene Co-expression Network Analysis (WGCNA), further revealed that the MEblue module exhibited a significant correlation with rutin content. This module includes *FtUF3GT1*, a gene that was found to co-express with multiple hub genes

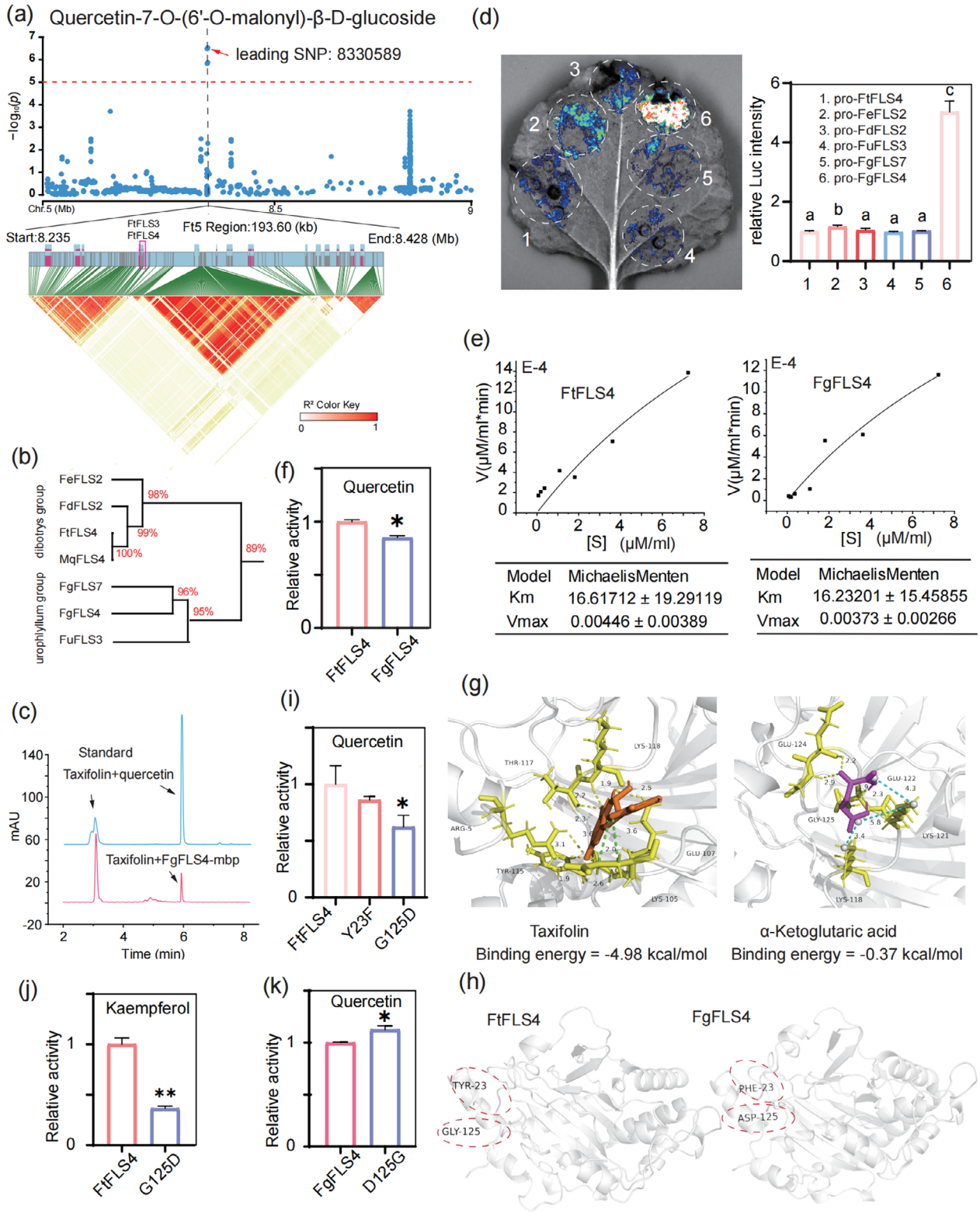

FIGURE 2 | Legend on next page.

FIGURE 2 | Functional comparison of FtFLS4 from *F. tataricum* and the homologous protein FgFLS4 from *F. gracilipes*. (a) Quercetin-7-O-(6′-O-malonyl)-β-D-glucoside GWAS in Tartary buckwheat accessions. (b) Similarity analysis of *FtFLS4* with homologous genes in different buckwheat varieties. (c) Enzymatic functionality verification of FgFLS4. (d) Comparison of the promoter activity of *FtFLS4* and its homologous genes, i.e., *FeFLS2*, *FdFLS2*, *FuFLS3*, *FgFLS7* and *FgFLS4*. (e) Enzyme kinetic constants of FtFLS4 and *FgFLS4*. (f) Relative activity of FtFLS4 and FgFLS4 under substrate saturation state with quercetin as a substrate. (g) Molecular docking of the FtFLS4 protein model with taxifolin and α-ketoglutarate. AlphaFold-predicted Q9ZWQ9.1.A structure as a template (with 73% sequence identity). Left: taxifolin; right: α-ketoglutarate. Green dashed lines indicate hydrophobic interactions, while yellow dashed lines indicate hydrogen bonds, with distances measured in Å. (h) Key differential sites between FtFLS4 and FgFLS4 proteins. (i) Relative activity with taxifolin as the substrate of FtFLS4 Y23F and G125D site mutations. (j) Relative activity with aromadendrin as substrate of the FtFLS4 G125D site mutation. (k) Relative activity with taxifolin as the substrate of the FgFLS4 D125G site mutation. $^{*}p < 0.05$, $^{**}p < 0.01$. One-way ANOVA and Tukey's post-test were used to calculate the significant differences relative to the control. Different letters indicate significant differences ($p < 0.05$), while the same letters denote no significant differences.

within the module (Figure S10, Table S4). These findings collectively highlight the MEblue module's strong connection to rutin accumulation in buckwheat.

FtUF3GT1 was shown to catalyse the synthesis of isoquercitrin (Huang et al. 2024; Zhang et al. 2021), a key precursor in the rutin biosynthesis pathway. While FtUF3GT1 directly produces isoquercitrin, its strong co-expression within a module highly correlated with rutin content strongly suggests that it plays a critical, indirect role in rutin biosynthesis by providing this essential intermediate. We further identified homologous proteins of FtUF3GT1 across diverse buckwheat varieties (Figure S11a), and these homologues consistently exhibited conserved catalytic functions (Figure S11b,c). To ascertain the functional importance of these homologues in different buckwheat species, we analysed their promoter activity and enzyme function. Compared with *FtUF3GT1*, the homologues *FgUF3GT19*, *FgUF3GT10* and *FuUF3GT5* exhibited extremely low promoter activity (Figure 3b). Notably, the *FtUF3GT1* promoter harbours a higher number of MRE (MYB recognition elements), which likely contributes to its strong UV-B responsiveness (Figures 3c and S11, Table S5), consistent with previous findings on UV-B-induced regulation of flavonoid biosynthesis (Liu et al. 2023). Functionally, FtUF3GT1 also demonstrated significantly stronger catalytic efficiency in isoquercitrin synthesis compared to FgUF3GT19 (Figure 3d).

Molecular docking analysis, combined with the identification of amino acid variations between FtUF3GT1 and FgUF3GT19, revealed that the T225P mutation in FtUF3GT1 led to decreased enzyme activity and a reduction in isoquercitrin and total flavonoid content in overexpressed hairy roots, without affecting its subcellular localization (Figure S12). In contrast, the corresponding P344T mutation in FgUF3GT19 had no significant effect on its catalytic activity (Figure S12j). This result suggests that the functional divergence between FtUF3GT1 and FgUF3GT19 is likely a result of the cumulative effect of multiple amino acid changes rather than a single residue.

Overall, *FtUF3GT1* demonstrates significantly superior promoter activity and catalytic capacity compared to its homologues, firmly establishing its central role in the higher rutin and isoquercitrin accumulation in Tartary buckwheat (Figure S12). However, a similar isoquercitrin level was also observed in *F. urophyllum* seeds, suggesting that *FtUF3GT1* homologues in *F. urophyllum* and *F. gracilipes* may not play a comparably dominant role in flavonoid biosynthesis in those species.

To identify additional *UF3GT* genes involved in flavonoid biosynthesis in buckwheat, we performed a comprehensive gene family analysis. Our findings revealed multiple copies of *UF3GT* genes across buckwheat varieties, with copy number variations among different cultivars (Figure S13a–c). However, these variations showed no significant correlation with either flavonoid content or UV-B response phenotypes (Figure S13d,e). Notably, the expression levels of *FtUF3GT1* and its homologues exhibited a significant positive correlation with seed rutin content (Figure S13e), highlighting their importance in rutin accumulation.

Gene copies are subject to evolutionary selective pressures (Wolfe and O'hUigín 2016; Yang et al. 2024). We therefore investigated which *UF3GT* genes among these copies might be under positive selection. When the branch containing *FtUF3GT1* was considered the background, adjacent branches showed evidence of significant positive selection (Figure 3e,f). Specifically, residues 302 and 314 K near the predicted active site of FdUF3GT2 were identified as potential positive selection sites, in contrast to 234 L and 222G in FtUF3GT1 (Figures 3g and S12). FdUF3GT2 from the foreground branch also exhibited the ability to catalyse isoquercitrin formation (Figure 3h). Our results demonstrate that isoquercitrin biosynthesis in buckwheat involves multiple *UF3GT* family members, and neither FtUF3GT1 nor its homologues are under recent strong positive selection. Intriguingly, when using the clade containing *FdUF3GT2* as the background branch and the branch harbouring *FtUF3GT5* (which shares segmental duplication with *FtUF3GT1*, Figure S6) as the foreground branch, we identified additional *UF3GT* genes under positive selection (Figure S13f,g). These findings provide compelling evidence that gene duplication and subsequent positive selection have collectively driven the functional diversification of *UF3GT* genes in buckwheat. Furthermore, comparative analyses suggest that more additional *UF3GT* genes contribute to isoquercitrin and rutin biosynthesis in *F. urophyllum* and *F. gracilipes*, complementing the role of *FtUF3GT1* in *F. tataricum*.

2.4 | Amino Acid Residues in the PGSG Box Influence Rutin Synthesis in Buckwheat

Rutin is a major flavonoid compound in buckwheat and is thought to contribute to the ecological adaptability of buckwheat (Kreft et al. 2022). Based on the metabolite GWAS dataset (Zhao et al. 2023), we identified a strong association between Malvidin-3-O-(6″-acetylglucoside)-5-glucoside

content and SNP 21933983 on chromosome 4, located approximately 30 kb away from *FtRT1*, indicating a region of high linkage (Figure 4a). Malvidin and rutin biosynthesis diverge after a common intermediate (aromadendrin) in the phenylpropanoid pathway (Luo et al. 2022). Furthermore, WGCNA analysis revealed that the MEblack module containing *FtRT1* showed correlation with rutin content, with one hub gene being correlated with *FtRT1* (Figure S10, Table S4). Indeed, FtRT1 has been previously shown to catalyse rutin formation (Zhao et al. 2024) and exhibits activity towards a broad range of substrates, including afzelin, astragalin, quercetin-7-O-β-D-glucopyranoside and hyperoside (Figure S14), indicating its

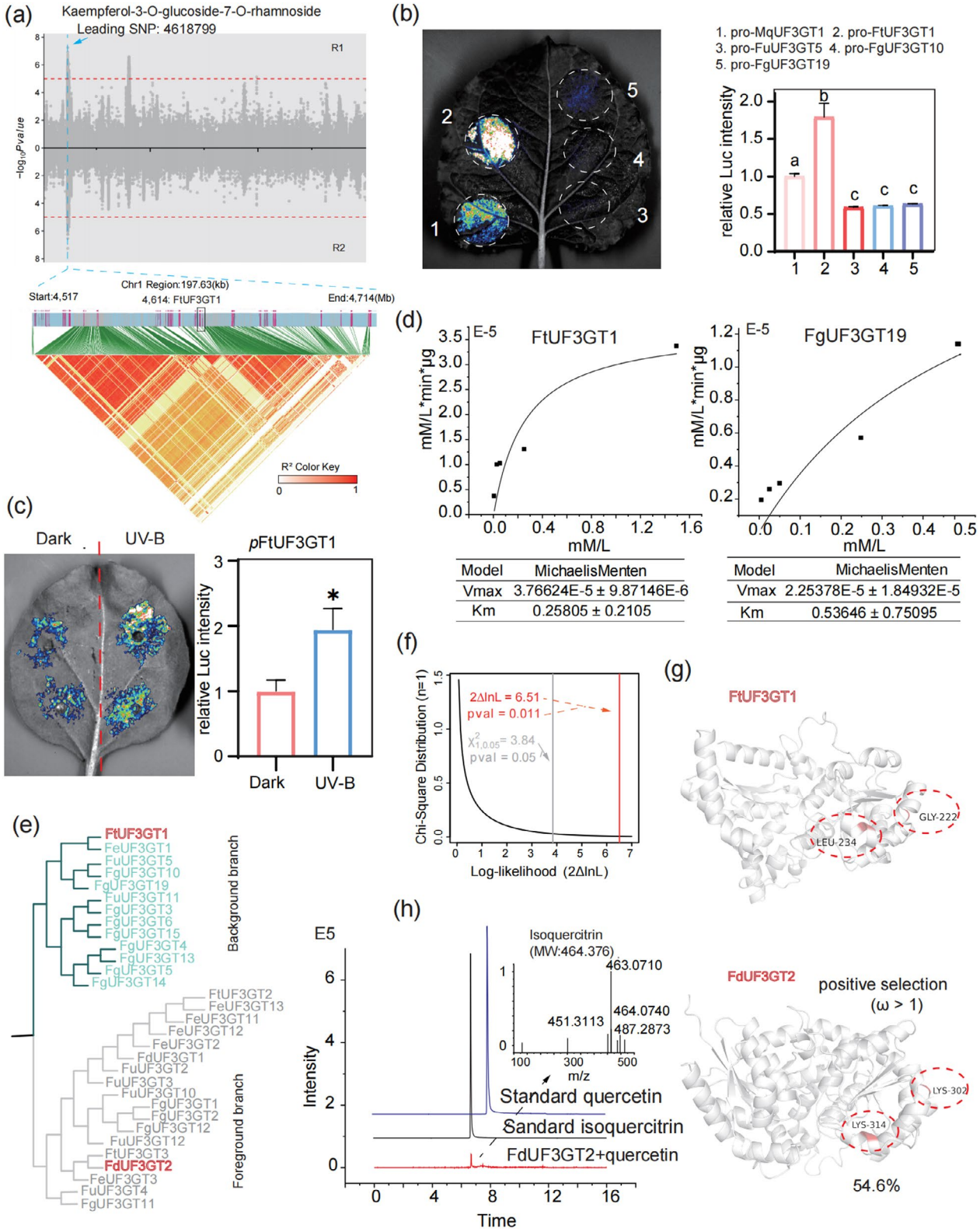

FIGURE 3 | Legend on next page.

FIGURE 3 | Analysis of key *UF3GT* genes involved in the formation of isoquercitrin in buckwheat. (a) Kaempferol-3-O-glucoside-7-O-rhamnoside GWAS in Tartary buckwheat accessions. (b) Comparison of the promoter activity of *FtUF3GT1* and its homologous *MqUF3GT1*, *FuUF3GT5*, *FgUF3GT10* and *FgUF3GT19*. (c) Promoter activity analysis of *FtUF3GT1* under UV-B treatment. 'Dark' indicates treatment with aluminium foil to exclude light. (d) Enzyme kinetic constants for *FtUF3GT1* and FgUF3GT19. (e) Phylogenetic tree showing foreground (containing *FdUF3GT2*) and background (containing *FtUF3GT1*) branches. Proteins highlighted in red are used for protein modelling. (f) Chi-square test distribution of significant positive selection in foreground branches. The red line indicates the significance of positive selection in foreground branches (p value = 0.011), where $2\Delta \ln L = 6.51$. The grey line indicates the significance threshold at p value = 0.05. (g) Visualisation of potential positive selection sites in Protein Models, with 54.6% indicating protein sequence similarity (modelled using AlphaFold-predicted structure A0A0A1H9W6.1.A as a template). (h) Functional validation of FdUF3GT2 with quercetin as substrate via UHPLC/MS. UHPLC (left) and mass spectrum (right) are shown. Electrospray ionisation is performed in negative ion mode. $^*p < 0.05$. One-way ANOVA and Tukey's post-test were used to calculate the significant differences relative to the control. Different letters indicate significant differences ($p < 0.05$), while the same letters denote no significant differences.

potential involvement in multiple branches of the phenylpropanoid pathway. Further gene family analysis revealed that *FtRT1* and its homologue *FeRT1* showed specific expression in seeds (Figure S15), suggesting their potential involvement in seed rutin synthesis.

To validate the function of RT homologues in buckwheat, we analysed their promoter and enzyme activities. Based on sequence similarity, FtRT1 homologues were classified into two groups, i.e., *cymosum* and *urophyllum* (Figure 4b). FgRT1 from the *urophyllum* group was also confirmed to catalyse rutin formation (Figure 4c). Promoter activity analysis revealed similar activity levels for most homologues, except for *FuRT3*, which exhibited lower activity (Figure 4d). This suggests that this group of homologues may have relatively stable expression in buckwheat to perform their functions, and the lower promoter activity of *FuRT3* might contribute to the lower rutin content observed in *F. urophyllum* compared to *F. tataricum*.

The significant differences in leaf flavonoid content between *F. tataricum* and *F. gracilipes*, as reported by Peng Dechuan et al. (2006), led us to compare the enzymatic functionality of FgRT1 (*urophyllum* group) and FtRT1 (*cymosum* group) under optimal catalytic conditions (Figure S16). FtRT1 exhibited higher Km and Vmax values compared to FgRT1 (Figure S17), with FgRT1 showing only 36% relative activity compared to FtRT1 (Figure 4e). Overexpression of *FgRT1* in hairy roots resulted in higher rutin content than the control but lower than *FtRT1* overexpression (Figure S18), indicating that the higher catalytic activity of FtRT1 may contribute to the higher rutin content in *F. tataricum* compared to *F. gracilipes*.

To identify the amino acid residues responsible for the differing catalytic activities, we conducted molecular docking and site-directed mutagenesis. These analyses highlighted the importance of the predicted active center and the conserved PGSG box for FtRT1 activity (Figures S19 and S20a). The PGSG box is a hallmark of glycosyltransferases (Vogt and Jones 2000). Within this motif, FtRT1 possesses ALA54, THR86 and ALA357, which differ from the corresponding SER56, ARG88 and VAL359 in FgRT1 (Figure 4f). Functional validation of FtRT1 mutants revealed that A54S, T86R and A357C resulted in decreased enzyme activities of 41%, 15% and 8%, respectively (Figure 4g). The A357C mutation, introducing a larger cysteine side chain compared to alanine, mirrors a similar ALA to CYS change observed in another buckwheat RT protein (Figure S20b). Hairy roots overexpressing these FtRT1 mutants (A357C-OE, T86R-OE and K53A-OE) showed decreased rutin synthesis and accumulation of upstream metabolites in the rutin synthesis pathway (Figures 4h and S20c). Alterations in FtRT1 function also appeared to affect its subcellular localization and cytoplasmic content (Figures 4i and S20d), potentially impacting its functionality. Conversely, in FgRT1, the S56V and R88T mutations had no significant effects, while the V359A mutation markedly increased enzyme activity by 61% (Figure 4j,k). Interestingly, the A357V mutation in FtRT1 had no observable effect on its function, whereas the A357C resulted in a functional change (Figure 4g), highlighting the subtle but significant influence of specific amino acid alterations. The aggregation of amino acids within the protein will form a hydrophobic microenvironment or various interactions (Lundberg and Borner 2019). Consequently, single amino acid substitutions can disrupt these interactions, leading to alterations in protein conformation (Kubo et al. 2004; Yang et al. 2023). Our identification of differential residues near ALA357 in FtRT1 and VAL359 in FgRT1 (Figure S21) underscores the potential for such localised variations to induce distinct geometric changes through synergistic effects with neighbouring amino acids, thereby elucidating the impact of PGSG box variations on RT enzyme functionality.

Finally, since UV-B radiation can enhance flavonoid synthesis (Xie et al. 2022), we investigated the transcriptional response of *FtRT1* and its homologues to UV-B treatment. Notably, only the *FtRT1* promoter (*pFtRT1*:LUC) exhibited significant activation under UV-B irradiation (Figure S22). This UV-B responsiveness was further confirmed in transgenic *Arabidopsis thaliana* harbouring the p*FtRT1*:GUS construct, which displayed enhanced GUS activity following UV-B exposure (Figure 4l). The presence of putative UV-B responsive elements like E-box and ACE-box within the *FtRT1* promoter (Figure S22) likely mediates this induction. Thus, the combination of higher intrinsic enzymatic activity and UV-B inducible promoter activity of *FtRT1* defines it as a key contributor to high rutin content and high-altitude adaptation in Tartary buckwheat.

2.5 | Enhanced Rutin-Related Metabolite Synthesis Confers UV-B Tolerance by Mitigating Oxidative Stress

Flavonoids, including rutin, act as molecular shields that mitigate UV-B-induced damage in plants (Kreft et al. 2022). To evaluate the functional contribution of rutin biosynthesis to UV-B tolerance, we analysed *FtFLS4-OE*, *FtUF3GT1-OE*

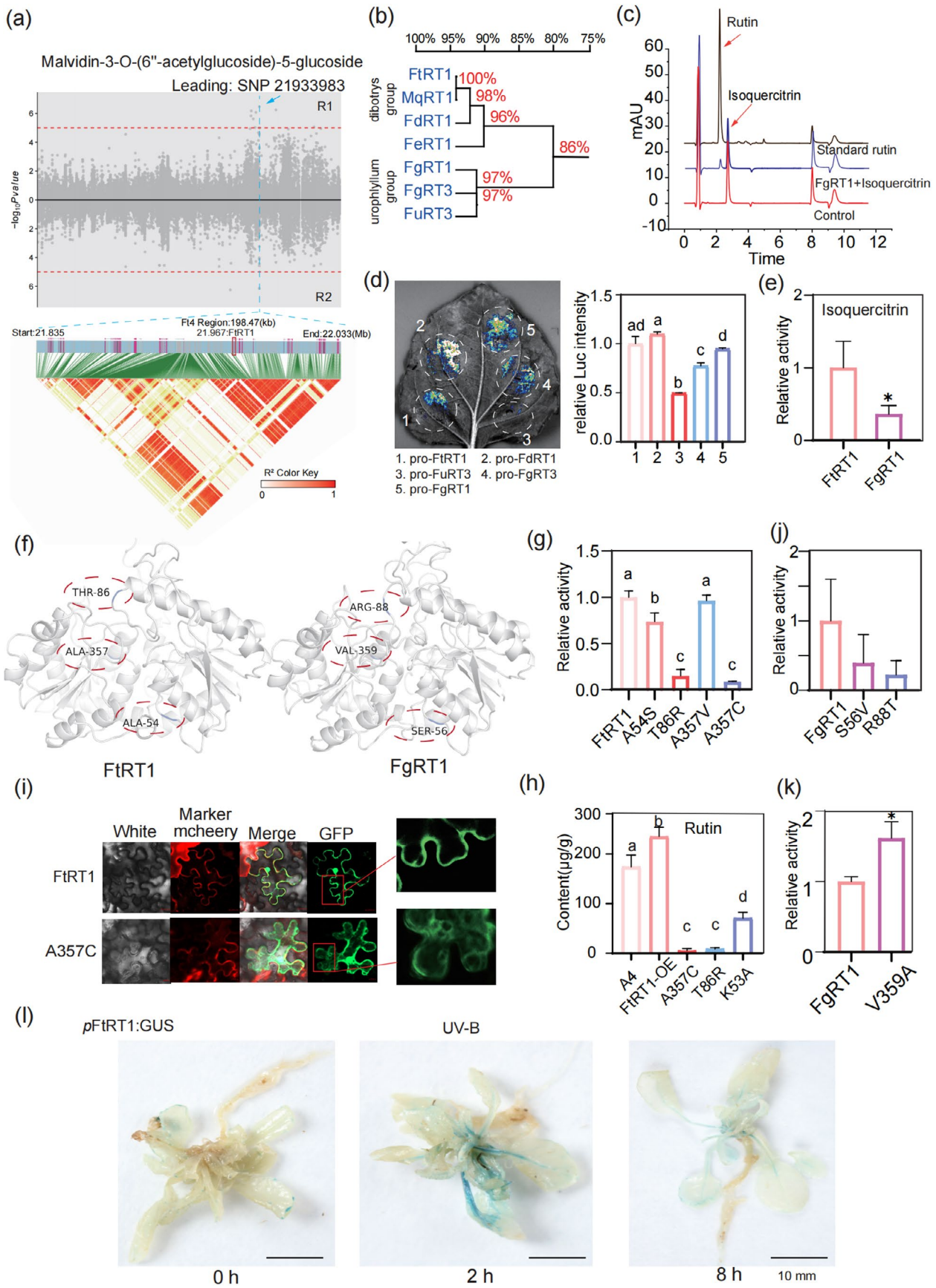

FIGURE 4 | Legend on next page.

FIGURE 4 | Catalytic properties of FgRT1 and FtRT1. (a) Malvidin-3-O-(6″-acetylglucoside)-5-glucoside GWAS in Tartary buckwheat accessions. (b) Similarity analysis of *FtRT1* with homologous genes in different buckwheat varieties. Genes are divided into two groups: The *cymosum* and *urophyllum* group. (c) UHPLC chromatogram showing the catalytic function of *FgRT1* taking isoquercitrin as a substrate, with control being His-tag purified from the *pET-28a* empty vector used for the enzyme reaction. (d) Comparison of the promoter activity of *FtRT1* and its homologous *FdRT1*, *FuRT3*, *FgRT3* and *FgRT1*. (e) Relative activity of FtRT1 and FgRT1, measured under substrate saturation state. (f) Key differential amino acid sites between FgRT1 and FtRT1. Both FtRT1 and FgRT1 were modelled using the X-ray–derived crystal structure 7erx.1.A as a template, with a sequence similarity greater than 30%, meeting modelling requirements. (g) Relative enzyme activity of FtRT1 key site mutations. The mutation sites of amino acid contain FtRT1 A54S, T86R,V and A357C. (h) Determination of rutin content in FtRT1-OE or site-muted *FtRT1*-OE (A357C-OE, T86R-OE, K53A-OE) hairy roots. (i) Subcellular localization of *FtRT1* A357C-GFP. (j) and (k) Relative enzyme activity of key site mutations (S56V, R88T, V359A) in FgRT1. Values are means ± SD ($n = 3$ biological replicates). $^*p < 0.05$. One-way ANOVA and Tukey's post-test were used to calculate significant differences relative to the control. Different letters indicate significant differences among groups ($p < 0.05$). (l) GUS staining of *FtRT1-promoter:GUS* transgenic *Arabidopsis*. 0 h indicates no UV-B treatment, while 2 and 8 h indicate UV-B treatment times.

and *FtRT1-OE* transgenic hairy roots and Arabidopsis lines. Under UV-B exposure, these overexpressed hairy roots and Arabidopsis lines exhibited significantly higher relative growth rates and increased lateral root development compared to controls (Figure 5a–c). Additionally, chlorophyll (a + b) content, typically reduced by UV-B stress (Chu et al. 2022), was significantly higher in all three overexpressed lines (Figure 5d–f), suggesting a protective role of flavonoids against UV-B-induced chlorophyll degradation.

Flavonoid accumulation in *A. thaliana* is responsive to environmental stimuli (Gatica-Arias et al. 2012; Misra et al. 2010). To correlate this enhanced tolerance with flavonoid accumulation, we quantified key metabolites in the *A. thaliana* overexpression lines. *FtFLS4-OE* plants showed elevated levels of isoquercitrin and quercetin, while *FtUF3GT1-OE* accumulated isoquercitrin and rutin. As expected, *FtRT1-OE* lines exhibited a significant increase specifically in rutin content (Figure S23a). Correspondingly, the total flavonoid content was significantly higher in *FtFLS4-OE* and *FtRT1-OE* lines, with a similar trend observed in *FtUF3GT1-OE* (Figure S23b). These results clearly demonstrate that overexpression of key rutin biosynthetic genes from Tartary buckwheat leads to increased accumulation of specific protective metabolites in *A. thaliana*.

Given the antioxidant properties of flavonoids in counteracting UV-B-induced ROS (Agati et al. 2012; Chen et al. 2022), we investigated ROS accumulation in our transgenic lines. Under non-stress conditions, ROS levels (detected by DAB and NBT staining for hydrogen peroxide and superoxide, respectively) were comparable between wild-type and overexpressed Arabidopsis. However, after UV-B exposure, wild-type plants showed a significant increase in hydrogen peroxide and superoxide levels, as evidenced by more intense staining. In contrast, the *FtFLS4-OE*, *FtUF3GT1-OE* and *FtRT1-OE* lines showed significantly reduced ROS accumulation under the same UV-B stress (Figure S23c). This compelling evidence indicates that the enhanced synthesis of rutin-related metabolites in the transgenic lines effectively mitigates UV-B-induced oxidative stress, thereby contributing to their increased tolerance.

3 | Discussion

The distribution of various buckwheat species, predominantly in high-altitude regions (Ohsako and Li 2020; Wen et al. 2021), underscores the importance of adaptive mechanisms to environmental stresses prevalent at these elevations, including elevated UV-B radiation. Flavonoids are well known to play a protective role in high-altitude adaptation (Kreft et al. 2022) and more specifically under UV-B exposure (Gu et al. 2022; Shi and Liu 2021; Solovchenko and Schmitz-Eiberger 2003). Our integrated approach combining UV-B phenotype assessments, in vivo metabolite profiling and exogenous flavonoid treatments provides clear evidence that flavonoids enhance UV-B tolerance (Figures 1, 5, S1, S2 and S23). A key focus of our investigation was to elucidate the genetic underpinnings of how variations in metabolite synthesis led to differential UV-B adaptation among buckwheat species. The core enzymes in rutin biosynthesis, *FLS*, *UF3GT* and *RT*, and their corresponding homologous proteins, exhibited greater sequence similarity within the *cymosum* group (*F. cymosum*, *F. tataricum* and *F. esculentum*) compared to the *urophyllum* group (*F. gracilipes* and *F. urophyllum*) (Figures S7, S13, and S15), a grouping consistent with established morphological and molecular classifications (Yasui and Ohnishi 1998). However, the levels of various rutin-related metabolites in *F. esculentum* were more comparable to those in *F. gracilipes* and *F. urophyllum* (Figure S1, Table S1), corroborating previous findings of significantly lower rutin-related metabolite content in *F. esculentum* compared to *F. tataricum* (Li et al. 2022; Zhang et al. 2023). This discrepancy highlights the complex interplay of metabolic pathways, as evidenced by the higher content of catechin, epicatechin, vitexin and isovitexin in *F. esculentum* (Figure S2), suggesting a metabolic flux directed away from rutin synthesis. Such intricate regulatory mechanisms of metabolite synthesis (Naik et al. 2022) likely play a crucial role in environmental adaptation (Li et al. 2024). Chromosomal synteny analysis further implicates genomic rearrangements in the spatial organisation and regulation of flavonoid biosynthesis genes (Figure S6), supporting the view that structural genome variation can affect gene expression and drive phenotypic divergence (Zhou et al. 2024; Raskina et al. 2008).

We focus on the genetic characteristics of flavonoid biosynthesis in different buckwheat species that contribute to UV-B adaptation, as well as the reasons for the distribution of *F. tataricum* at altitudes of 4500 m. The stability of promoter activity is fundamental to maintaining stable gene expression levels and phenotypes (Xue et al. 2023). Notably, the stable promoter activity of *FtFLS4* and *FtRT1* in the *cymosum* and *urophyllum* groups (Figures S2, S4) indicates that post-transcriptional factors, such as enzyme activity, play a larger role in determining metabolite

accumulation. The established role of *FLS* overexpression in enhancing stress resistance (Wang, Zhang, et al. 2021) and the phenotypic alterations resulting from *FLS* loss of function (Saxena et al. 2023) underscore the significance of this enzyme. Our comparative analysis revealed that the G125D mutations in *FtFLS4* and *FgFLS4* modulate enzyme functionality

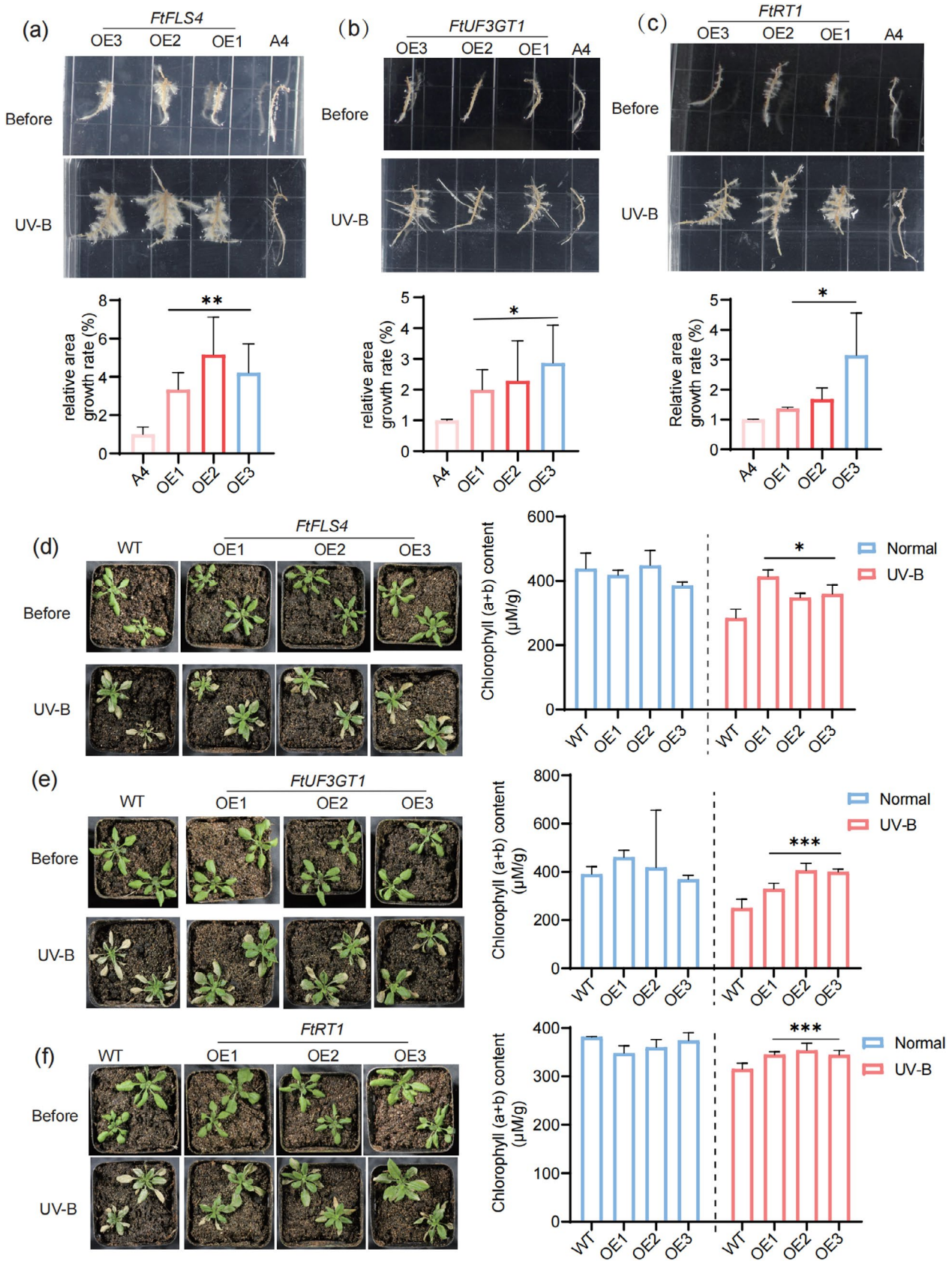

FIGURE 5 | Legend on next page.

FIGURE 5 | Overexpression of *FtFLS4*, *FtUF3GT1* and *FtRT1* enhances the resistance of *Arabidopsis* and hairy roots to UV-B radiation. (a) UV-B phenotype of *FtFLS4*-OE hairy roots (top) and relative growth area (bottom). (b) UV-B phenotype of *FtUF3GT1*-OE hairy roots (top) and relative growth area (bottom). (c) UV-B phenotype of *FtRT1*-OE hairy roots (top) and relative growth area (bottom). A4 serves as the control. (d) UV-B phenotype of *FtFLS4*-OE *Arabidopsis* (left) and chlorophyll (a + b) content (right). (e) UV-B phenotype of *FtUF3GT1*-OE *Arabidopsis* (left) and chlorophyll (a + b) content (right). (f) UV-B phenotype of *FtRT1*-OE *Arabidopsis* (left) and chlorophyll (a + b) content (right). Mean ± SD ($n = 3$ biological replicates). One-way ANOVA was used to calculate significant differences relative to the control, $^{*}p < 0.05$, $^{**}p < 0.01$, $^{***}p < 0.001$.

and the accumulation of quercetin and kaempferol (Figures 2, S8). However, the relatively subtle impact of these changes suggests a mechanism by which the *urophyllum* group maintains a baseline level of flavonoid synthesis. Interestingly, despite high promoter activity, *FgFLS4* in the *urophyllum* group did not lead to increased quercetin and kaempferol levels but rather an accumulation of quercitrin (Figure S1), potentially due to species-specific regulatory mechanisms of metabolite synthesis (Kang et al. 2014; Olarte et al. 2019). The differential UV-B responses observed for the *F. gracilipes* tetraploid (*FgFLS4* and *FgFLS7*; Figure S9) align with its broad altitudinal distribution (Wen et al. 2021), suggesting a complex regulatory landscape.

The conserved PGSG box in *RT* is critical for glycosyltransferase function, and variations within this motif can alter enzyme activity (Jadhav et al. 2012), impacting overall metabolic flux (Wu et al. 2023; Grubb et al. 2014). Our findings indicate that amino acid changes in the PGSG box of the *urophyllum* group *RT* homologues do not completely abolish enzyme function, allowing for residual rutin synthesis (Figure 4). Such natural variations affecting enzymatic activity can lead to altered flavonoid accumulation and consequently influence plant phenotypes, as demonstrated by *OsUGT707A2* in rice affecting apigenin 5-O-glucoside accumulation and resistance to UV-B (Peng et al. 2017). We propose that the variations in rutin content among buckwheat species due to PGSG box modifications contribute to their differential UV-B resistance. Furthermore, the UV-B-induced flavonoid accumulation, particularly the induction of *FtRT1* in the *cymosum* group (Figure 4), represents a crucial adaptive strategy for mitigating UV-B stress (Zhang et al. 2020), a response not observed in the *urophyllum* group.

Chromosomal rearrangements can influence chromatin accessibility and contact, potentially leading to differential expression of homologous genes across species (Wang, Jia, et al. 2021). The stark differences in expression level and promoter activity observed for *FtUF3GT1* and its *urophyllum* group homologues (Figure 3) may be attributed to such rearrangements within the *UF3GT* gene locus (Figure S6). However, this does not fully explain the similar isoquercitrin levels in *F. urophyllum* and *F. tataricum* (Figure 1), highlighting the complexity of plant metabolite synthesis, where a single enzyme's function can impact multiple compounds due to broad substrate recognition (Wang et al. 2023), and variations in multiple enzymes can lead to diverse metabolic outcomes (Yu et al. 2017). Moreover, the accumulation of intermediate metabolites is a balance of their synthesis and consumption (Gu et al. 2010). Therefore, we speculate that the comparable isoquercitrin levels in *F. urophyllum* result from the coordinated action of *FLS*, *UF3GT* and *RT*. Furthermore, we identified additional enzymes capable of catalysing isoquercitrin formation beyond *FtUF3GT1* and its direct homologues (Figure 3), with potential contributions from multiple enzymes in *F. urophyllum*, evidenced by gene copy number and selection pressure analysis (Figures 3 and S13). The relatively high expression of *FuFLS2* and the relatively low expression and catalytic capacity of *FuRT3* in *F. urophyllum* (Figures 4 and S7) may further contribute to isoquercitrin accumulation. Notably, *F. urophyllum*'s strong UV-B resistance (Figure 1) is associated with this isoquercitrin accumulation. Furthermore, the rigid branches characteristic of *F. urophyllum*, potentially linked to lignin synthesis, which also contributes to UV-B resistance (Gu et al. 2010; Hilal et al. 2004; McInnes et al. 2023), suggest unique adaptive mechanisms in this species.

In conclusion, our study provides compelling evidence for the crucial role of flavonoids in UV-B adaptation and identifies the enhanced functions of *FtFLS4*, *FtUF3GT1* and *FtRT1* in Tartary buckwheat, coupled with their promoters' responsiveness to UV-B, as key factors contributing to its high-altitude adaptation. These findings offer a valuable foundation for future research aimed at enhancing plant stress resistance through targeted metabolic engineering strategies.

4 | Materials and Methods

4.1 | Plant Materials and Treatments

Five *Fagopyrum* species, including *F. tataricum* (cv. Pinku and cv. Miqiao were selected as internal controls), *F. esculentum*, *F. cymosum*, *F. urophyllum* and *F. gracilipes*, were utilised for phenotypic assessment and metabolite content determination. The seeds were germinated in a plant tissue culture incubator (Model TCC800, Fujian Jiupo Biotechnology Co. Ltd., China) at 25°C. Seedlings were subjected to daily 8-h UV-B treatment to induce stress, while the control group received methanol. For the metabolite treatment experiment, the following metabolites were simultaneously administered to seedlings under UV-B irradiation (by UV-B lamp) at specific final concentrations, including 1 mM cinnamic acid, 1 mM procyanidin, 5 mM isoquercitrin, 10 mM rutin, 5 mM kaempferol, 5 mM quercetin, 2.5 mM 4-(Dimethylamino) cinnamaldehyde, 5 mM apigenin, 5 mM cyanidin and 5 mM nicotiflorin.

The seeds of *Brassica oleracea*, *Glycine max*, *Vigna radiata*, *Triticum aestivum*, *Oryza sativa* and *Hordeum vulgare* were used for cross-species UV-B phenotype evaluation. Rice was germinated at 37°C, while other species were germinated under ambient temperature and exposed to UV-B.

4.2 | Metabolite Content Determination

Dried seeds and freeze-dried plant tissues were ground into powder. Metabolites were extracted by ultrasonicating 0.1 g of this powder in 80% (v/v) methanol for 50 min. Extracts were filtered through

a nylon membrane and analysed using Ultra-High Performance Liquid Chromatography (UHPLC) coupled with a fast triple quadrupole mass spectrometry (LC-QqQ-MS/MS) approach (Lai et al. 2025). A Waters X Select HSS T3 column (2.1 mm × 100 mm × 1.8 μm) coupled with a 6490 Triple Quadrupole LC/MS System (ESI-triple quadrupole-linear ion trap (QTRAP)-MS) was utilised in UHPLC for qualitative and quantitative analysis of metabolites. The UHPLC gradient was 98% water/2% acetonitrile (0–4 min), linear gradient to 5% water/95% acetonitrile (4–11 min), linear gradient to 80% water/20% acetonitrile (11–13 min) and return to 98% water/2% acetonitrile (13–15 min). Three biological replicates were analysed per sample. However, the methanol extract was mixed with 0.1 mol/L $AlCl_3$ and 1 mol/L CH_3COOK, and absorbance was measured at 420 nm using a Synergy HTX Multi-Mode Microplate Reader (BioTek, USA).

4.3 | Genome-Wide Association Study

The metabolic content data of 200 core accessions of tartary buckwheat were obtained from Zhao et al. (2023). Genome-wide association study (GWAS) on flavonoid metabolite content in Tartary buckwheat (*Fagopyrum tataricum*) was performed using the factorial spectral transform linear mixed model (FaST-LMM). Manhattan plots were generated using the CMplot package in R software. Candidate genes were identified within a 100-kb flanking region surrounding significant loci, as determined by the whole-genome linkage disequilibrium (LD) decay distance.

4.4 | Gene Family and Phylogenetic Analysis

Genomic data for the five *Fagopyrum* species were downloaded from the Buckwheat Genome Project Database (GPDB) (http://47.93.16.146/home#/home). Protein functional annotations were predicted using EggNog-mapper (Huerta-Cepas et al. 2019), and Blastp was used for comparisons against GO, KEGG, DOG, NR and SwissProt databases. Known sequences of flavonoid biosynthetic genes *FLS* (Li et al. 2012), *UF3GT* (Huang et al. 2024) and *RT* (Zhao et al. 2024) from *F. tataricum* were aligned to identify homologous sequences across different buckwheat species.

Phylogenetic trees of *FtFLS*, *FtUF3GT* and *FtRT* were constructed using the maximum likelihood method in IQ-TREE (v1.6.12) with the JTT + G4 model and 1000 bootstrap replicates (Sleator 2016). *Rheum palmatum* homologous sequences served as the outgroup. Chromosome distribution was visualised using TBtools, and synteny analysis was performed using the Python Multiple Collinear Scanning toolkit (JCVI) (Sleator 2016). Transcriptome data for Tartary buckwheat, common buckwheat and golden buckwheat were obtained from publicly available sources (He et al. 2022; He et al. 2023; Zhang et al. 2017).

4.5 | Total RNA Isolation, cDNA Synthesis and qRT-PCR

RNA was extracted from one-week-old seedlings of *F. tataricum* cv. Pinku, *F. tataricum* cv. Miqiao, *F. esculentum*, *F. urophyllum* and *F. gracilipes* and leaf tissues of *F. cymosum* (due to lack of viable seeds) using the RNAprep Pure Plant Total RNA Extraction Kit (TIANGEN, China). The cDNA was synthesised using the HiScript II 1st Strand cDNA Synthesis Kit (Vazyme, China).

Quantitative Real-time polymerase chain reaction (qRT-PCR) was conducted with Taq Pro Universal SYBR qPCR Master Mix on a BIO-RAD CFX96 real-time PCR system (Bio-Rad Laboratories, Hercules, CA, USA) using primers listed in Table S6. The $2^{-\Delta\Delta CT}$ method (Livak and Schmittgen 2001) was employed for data analysis.

4.6 | Promoter Activity Analysis

The 1000 bp promoter sequences of *FLS*, *UF3GT* and *RT* were cloned into the pGreenII 0800-LUC vector (Table S6) and transformed into *Agrobacterium tumefaciens* strain GV3101 (ZOMANBIO, Beijing, China). Positive GV3101 cells were resuspended in MES buffer (0.2 mM MES, 1 mM $MgCl_2$ and 0.1 mM acetosyringone), and agroinfiltration was performed in tobacco leaves, followed by dual-luciferase reporter assays. After two days, fluorescence imaging was observed using the Tanon 5200 luminescence imaging system. LUC intensity was measured using the Dual Luciferase Reporter Assay Kit (Vazyme, China). To assess the induction of promoter activity by UV-B treatment, half of each infiltrated leaf was covered with aluminium foil (control), while the other half was exposed to UV-B for 3 h (Leonardelli et al. 2024).

4.7 | Molecular Docking and Site-Directed Mutagenesis

Protein modelling was performed using SWISS-MODEL (Waterhouse et al. 2018), and 3D structures of small molecular compounds were obtained from the National Center for Biotechnology Information (NCBI) (https://pubchem.ncbi.nlm.nih.gov/). Molecular docking of proteins and small molecules was performed using AutoDockTools-1.5.7, and the docking results were visualised using PyMOL (Lam and Siu 2017). Site-directed mutagenesis was performed using specific primers (Table S6) to introduce mutations into the protein sequences.

4.8 | Enzyme Activity Assays

FLS and *UF3GT* genes were cloned into the pMAL-c5X vector, and *RT* was cloned into the pET-28a (+) vector (primers in Table S6) and expressed in *E. coli* BL21 competent cells (ZOMANBIO, China) for protein purification. Proteins were purified using ultrasonic cell disruption in extraction buffer (50 mM Tris, 150 mM NaCl, pH 7.6), followed by affinity chromatography using Ni-NTA agarose (Thermo Fisher Scientific, USA) and MBPSep Dextrin Agarose Resin 6FF (Yeasen, China). MBP-tagged proteins were eluted with Elution buffer 1 (50 mM Tris, 150 mM NaCl, 20 mM maltose, pH 7.6), and His-tagged proteins were eluted with Elution buffer 2 (50 mM Tris, 150 mM NaCl, 200 mM imidazole, pH 7.6). Purified proteins were quantified using the Bradford Quick Protein Quantification Kit (ZOMANBIO, China) and stored at −80°C.

To evaluate enzyme functionality, catalytic reactions were conducted in 50 mM Tris-HCl buffer (pH 7.6), containing 50 mM Fe_2SO_4, 10 mM L-ascorbic acid and 50 mM 2-ketoglutaric acid, with either 10 mM aromadendrin or 10 mM taxifolin as substrates and 10 μg of FLS protein. For UF3GT enzyme activity assays, 10 μg of UF3GT protein was incubated with 10 mM quercetin, 20 mM UDP-glucose and 1 mM dithiothreitol (DTT) in a total volume of 200 μL. RT enzyme assays were performed using 10 μg of RT protein with 10 mM of each substrate, including isoquercitrin, astragalin, hyperoside, quercetin-7-O-β-D-glucopyranoside and afzelin, along with 20 mM UDP-glucose, 1 mM $MgCl_2$ and 1 mM DTT. Enzyme kinetic constants were determined by varying substrate concentrations.

The optimal pH was evaluated using the buffers of 50 mM CH_3COONa (pH 3.0–4.5), 50 mM KH_2PO_4 (pH 6.0), 50 mM Tris–HCl (pH 7.0–9.0) and Na_2CO_3 (pH 10.0–12.0). Optimal temperatures were tested at 4°C, 16°C, 30°C, 37°C and 65°C, and reactions were sampled at 0.05, 1, 5, 30, 60 and 720 min. All reaction products were freeze-dried, re-dissolved in methanol, filtered and stored at −80°C. Enzyme kinetics were measured using UHPLC-CAD/DAD (Thermo Vanquish F, USA), and the enzyme activity of FdUF3GT2 was further validated using nanoLC-QTOF (Agilent, USA).

4.9 | Subcellular Localization

FLS, *UF3GT*, *RT* and their corresponding mutant sequences were cloned into the pCAMBIA1305-GFP vector (primer sequences listed in Table S6) and introduced into *Agrobacterium tumefaciens* strain GV3101. For subcellular localisation analysis, agroinfiltration was performed on tobacco leaves, followed by one day of dark incubation and one day of light exposure, after which GFP fluorescence was visualised using a Zeiss LSM900 Laser Scanning Confocal Microscope.

4.10 | Construction of Overexpressed Materials

FLS, *UF3GT* and *RT* sequences were individually cloned into the pCAMBIA 1307-cmyc vector under the control of the CaMV 35S promoter with a Myc-tag using primers listed in Table S6. These homologous recombination vectors were then transformed into *A. tumefaciens* strain GV3101 and *A. rhizogenes* strain A4 (ZOMANBIO, Beijing, China). Four-week-old *A. thaliana* (Col-0) plants were transformed via the floral dip method using GV3101 carrying the overexpression constructs by resuspending the bacterial suspension in 5% sucrose solution containing 0.05% Silwet77 (Chen and Murata 2002). Arabidopsis seeds were surface-sterilised with 75% ethanol for 10 min, followed by 100% ethanol for another 10 min and then air-dried. Transgenic seeds were selected on MS solid medium containing hygromycin B.

For hairy root transformation, A4 strain was resuspended in liquid MS medium (3% sucrose, pH 5.8) and used to infect three-week-old buckwheat explants. Transformed hairy roots were selected on MS solid medium containing hygromycin.

Genomic DNA was extracted from eight-week-old Arabidopsis leaves and hairy roots using the CTAB method (Schenk et al. 2023). The presence of the transgene was confirmed by PCR using primers from the pCAMBIA 1307-cmyc vector (as listed in the Table S6). For protein identification in hairy roots, total protein was extracted using a plant protein extraction buffer (100 mM Tris, 250 mM NaCl, 1 mM DTT, 0.05% β-mercaptoethanol, Roche cOmplete Protease Inhibitor Cocktail, pH 7.5) after grinding the plant tissue in liquid nitrogen. Western Blotting was used to check for positive hairy roots. Myc Tag antibody (Thermo Fisher, USA) was taken as the first antibody. Mouse Anti-Goat IgG antibody (Bioss, China) was taken as the second antibody, followed by washing and detection. The detection solution used was Immobilon Western Chemiluminescent HRP Substrate (Millipore, USA), and imaging was performed using the Tanon 5200 luminescence imaging system (Figure S24).

4.11 | Hairy Root UV-B Treatment

Hairy root tips with meristematic regions were transferred to MS solid medium for two days before initial images were taken. Roots were then treated with daily 8-h UV-B exposure for two weeks, followed by post-treatment imaging.

Six-week-old Arabidopsis plants were imaged initially and then exposed to daily 16-h UV-B treatment until phenotypic changes were observed.

4.12 | GUS Staining

The *FtRT1* promoter sequence was cloned into the pCAMBIA1391 vector (primers in Table S6) to create a Promoter-*FtRT1*:GUS construct. This construction was introduced into six-week-old Arabidopsis via floral dip transformation, and positive seedlings were selected on hygromycin B-containing MS solid medium. GUS staining was performed on these seedlings after UV-B exposure at different time points.

4.13 | Chlorophyll Content Measurement and DAB Staining

Chlorophyll (a + b) content was measured in Arabidopsis leaves by extracting pigments in a solution of 85% acetone and 100 mM Tris (pH 8.0), followed by a fivefold dilution with 80% acetone (Chazaux et al. 2022). Absorbance was read at 663.6 nm and 646.6 nm using a Synergy HTX Multi-Mode Microplate Reader (BioTek, USA). The calculations were performed according to the protocols used by Chazaux et al. (2022).

Hydrogen peroxide detection in plant tissues was performed using diaminobenzidine (DAB) solution (10 mM Tris, 0.1% DAB, pH 7.6), followed by decolorization with 85% ethanol and 15% acetic acid.

4.14 | Positive Selection Analysis

The CODEML program from the PAML software package was used to calculate the ratio of nonsynonymous (dN) to

synonymous (dS) substitution rates ($\omega = dN/dS$) to detect positive selection. Maximum Likelihood methods were used to compare null and alternative hypotheses. The Chi-square test assessed the significance of positive selection. The branch-site model was employed to identify amino acid sites under positive selection ($\omega > 1$) in specific branches.

4.15 | Weighted Gene Co-Expression Network Analysis

WGCNA was performed using transcriptomic data from different buckwheat tissues coupled with metabolomics (Hou et al. 2021) focusing on key flavonoid metabolites (including rutin, quercetin, isoquercitrin, astragalin, kaempferol, aromadendrin and taxifolin). The transcriptome data were obtained from Buckwheat Genome Project Database (GPDB) (http://47.93.16.146/home#/home). Co-expression networks between hub genes and target genes were visualised using Cytoscape software.

4.16 | Statistical Analysis

Histograms were plotted using Origin 2019b. All the box and column diagrams were obtained by GraphPad Prism 10 software. Significant differences between two groups were assessed using two-tailed Student's *t*-test. For comparisons of multiple groups, one-way analysis of variance (ANOVA) was performed. Significance levels were defined as $^{*}p < 0.05$; $^{**}p < 0.01$; and $^{***}p < 0.001$.

Author Contributions

M.Z. designed and managed the project. M.Z. and K.Z. organised the funding for this research. M.Z. and K.Z. provided the genetic materials. Y.G., T.J., C.M., M.N.H. and W.L. performed most of the experiments. Y.G., L.H. and Y.S. performed the bioinformatics analysis. Y.G., T.J., Y.S. and M.N.H. performed data analysis and figure design. Y.G., T.J., M.N.H., H.C., A.R.F., Y.H. and M.Z. wrote the manuscript. All authors read and approved the manuscript.

Acknowledgements

Thanks to the public laboratory of the Biotechnology Research Institute, Chinese Academy of Agricultural Sciences for use of the HPLC and triple-quadrupole MS/MS instrument. We are grateful for the Institute of Crop Sciences, Chinese Academy of Agricultural Science, Yufei Wang for providing the dicotyledonous seeds. This work was supported by the National Natural Science Foundation of China (32241038).

Conflicts of Interest

The authors declare no conflicts of interest.

Data Availability Statement

The datasets generated and analyzed in this study are publicly available through the following repositories: (1) Raw sequencing data have been deposited in the China National Center of Bioinformation (CNCB) under accessions PRJCA009421 (DOI: 10.1111/nph.18306), PRJCA010349 (DOI: 10.1111/jipb.13459), and PRJCA009237 (DOI: 10.1016/j.molp.2017.08.013); (2) Wild buckwheat genomic resources are accessible via the Buckwheat Genome and Phenome Database (BuckwheatGPDB) at http://47.93.16.146/.

References

Agati, G., E. Azzarello, S. Pollastri, and M. Tattini. 2012. "Flavonoids as Antioxidants in Plants: Location and Functional Significance." *Plant Science* 196: 67–76.

Bright, L. J., J. F. Gout, and M. Lynch. 2017. "Early Stages of Functional Diversification in the Rab GTPase Gene Family Revealed by Genomic and Localization Studies in Paramecium Species." *Molecular Biology of the Cell* 28: 1101–1110.

Chazaux, M., C. Schiphorst, G. Lazzari, and S. Caffarri. 2022. "Precise Estimation of Chlorophyll a,b and Carotenoid Content by Deconvolution of the Absorption Spectrum and New Simultaneous Equations for Chl Determination." *Plant Journal* 109: 1630–1648.

Chen, T. H. H., and N. Murata. 2002. "Enhancement of Tolerance of Abiotic Stress by Metabolic Engineering of Betaines and Other Compatible Solutes." *Current Opinion in Plant Biology* 5: 250–257.

Chen, Z. R., Y. Dong, and X. Huang. 2022. "Plant Responses to UV-B Radiation: Signaling, Acclimation and Stress Tolerance." *Stress Biology* 2: 51.

Chu, R., Q. H. Zhang, and Y. Z. Wei. 2022. "Effect of Enhanced UV-B Radiation on Growth and Photosynthetic Physiology of *Iris tectorum* Maxim." *Photosynthesis Research* 153: 177–189.

Danino, Y. M., D. Even, D. Ideses, and T. Juven-Gershon. 2015. "The Core Promoter: At the Heart of Gene Expression." *BBA Gene Regulatory Mechanisms* 1849: 1116–1131.

Gatica-Arias, A., M. A. Farag, M. Stanke, J. Matousek, L. Wessjohann, and G. Weber. 2012. "Flavonoid Production in Transgenic Hop (*Humulus lupulus* L.) Altered by PAP1/MYB75 From *Arabidopsis thaliana* L." *Plant Cell Reports* 31: 111–119.

Gillani, M., and G. Pollastri. 2024. "Protein Subcellular Localization Prediction Tools." *Computational and Structural Biotechnology Journal* 23: 1796–1807.

Golob, A., N. Luzar, I. Kreft, and M. Germ. 2022. "Adaptative Responses of Common and Tartary Buckwheat to Different Altitudes." *Plants* 11: 1439.

Grubb, C. D., B. J. Zipp, J. Kopycki, et al. 2014. "Comparative Analysis of *Arabidopsis* UGT74 Glucosyltransferases Reveals a Special Role of UGT74C1 in Glucosinolate Biosynthesis." *Plant Journal* 79: 92–105.

Gu, M. L., J. Yang, X. Tian, W. M. Fang, J. P. Xu, and Y. Q. Yin. 2022. "Enhanced Total Flavonoid Accumulation and Alleviated Growth Inhibition of Germinating Soybeans by GABA Under UV-B Stress." *RSC Advances* 12: 6619–6630.

Gu, X. D., M. Y. Sun, L. Zhang, et al. 2010. "UV-B Induced Changes in the Secondary Metabolites of *Morus alba* L." *Molecules* 15: 2980–2993.

Häder, D. P., and N. A. Cabrol. 2020. "Monitoring of Solar Irradiance in the High Andes." *Photochemistry and Photobiology* 96: 1133–1139.

He, M., Y. He, K. Zhang, et al. 2022. "Comparison of Buckwheat Genomes Reveals the Genetic Basis of Metabolomic Divergence and Ecotype Differentiation." *New Phytologist* 235: 1927–1943.

He, Q., D. Ma, W. Li, et al. 2023. "High-Quality Genome Provides Insights Into the Flavonoid Accumulation Among Different Tissues and Self-Incompatibility." *Journal of Integrative Plant Biology* 65: 1423–1441.

Hilal, M., M. F. Parrado, M. Rosa, et al. 2004. "Epidermal Lignin Deposition in Quinoa Cotyledons in Response to UV-B Radiation." *Photochemistry and Photobiology* 79: 205–210.

Hou, S., W. Du, Y. Hao, et al. 2021. "Elucidation of the Regulatory Network of Flavonoid Biosynthesis by Profiling the Metabolome and

Transcriptome in Tartary Buckwheat." *Journal of Agricultural and Food Chemistry* 69: 7218–7229.

Hsieh, K., and A. H. C. Huang. 2007. "Tapetosomes in Tapetum Accumulate Endoplasmic Reticulum-Derived Flavonoids and Alkanes for Delivery to the Pollen Surface." *Plant Cell* 19: 582–596.

Huang, X., Y. Q. He, K. X. Zhang, et al. 2024. "Evolution and Domestication of a Novel Biosynthetic Gene Cluster Contributing to the Flavonoid Metabolism and High-Altitude Adaptability of Plants in the *Fagopyrum* Genus." *Advanced Science* 11: 2403603.

Huerta-Cepas, J., D. Szklarczyk, D. Heller, et al. 2019. "eggNOG 5.0: A Hierarchical, Functionally and Phylogenetically Annotated Orthology Resource Based on 5090 Organisms and 2502 Viruses." *Nucleic Acids Research* 47: D309–D314.

Jadhav, S. K. R., K. A. Patel, B. B. Dholakia, and B. M. Khan. 2012. "Structural Characterization of a Flavonoid Glycosyltransferase From." *Bioinformation* 8: 943–949.

Kang, J. H., J. McRoberts, F. Shi, J. E. Moreno, A. D. Jones, and G. A. Howe. 2014. "The Flavonoid Biosynthetic Enzyme Chalcone Isomerase Modulates Terpenoid Production in Glandular Trichomes of Tomato." *Plant Physiology* 164: 1161–1174.

Körner, C. 2007. "The Use of 'Altitude' in Ecological Research." *Trends in Ecology & Evolution* 22: 569–574.

Kreft, I., A. Vollmannova, J. Lidikova, et al. 2022. "Molecular Shield for Protection of Buckwheat Plants From UV-B Radiation." *Molecules* 27: 5577.

Kubo, A., Y. Arai, S. Nagashima, and T. Yoshikawa. 2004. "Alteration of Sugar Donor Specificities of Plant Glycosyltransferases by a Single Point Mutation." *Archives of Biochemistry and Biophysics* 429: 198–203.

Lai, D., Y. Fan, M. Nurul Huda, et al. 2025. "Development of a Fast LC-QqQ-MS/MS Method for Detecting Flavonoids in the Phenylpropanoid Pathway of Plants." *Journal of Integrative Agriculture* 24: 5.

Lai, D., K. Zhang., Y. He, et al. 2024. "Multi-Omics Identification of a Key Glycosyl Hydrolase Gene FtGH1 Involved in Rutin Hydrolysis in Tartary Buckwheat (*Fagopyrum tataricum*)." *Plant Biotechnology Journal* 22: 1206–1223.

Lam, W. W. T., and S. W. I. Siu. 2017. "PyMOL mControl: Manipulating Molecular Visualization With Mobile Devices." *Biochemistry and Molecular Biology Education* 45: 76–83.

Leonardelli, M., N. Tissot, R. Podolec, et al. 2024. "Photoreceptor-Induced Sinapate Synthesis Contributes to Photoprotection in *Arabidopsis*." *Plant Physiology* 196: 1518–1533.

Li, C. L., Y. C. Bai, S. J. Li, et al. 2012. "Cloning, Characterization, and Activity Analysis of a Flavonol Synthase Gene and Its Association With Flavonoid Content in Tartary Buckwheat." *Journal of Agricultural and Food Chemistry* 60: 5161–5168.

Li, H. R., Y. X. Li, H. Deng, et al. 2018. "Tomato UV-B Receptor SlUVR8 Mediates Plant Acclimation to UV-B Radiation and Enhances Fruit Chloroplast Development via Regulating SlGLK2." *Scientific Reports* 8: 6097.

Li, H. Y., Q. Y. Lv, A. Liu, et al. 2022. "Comparative Metabolomics Study of Tartary (*Fagopyrum tataricum* (L.) Gaertn) and Common (*Fagopyrum esculentum* Moench) Buckwheat Seeds." *Food Chemistry* 371: 131125.

Li, J., P. Yang, Q. H. Yang, et al. 2019. "Analysis of Flavonoid Metabolites in Buckwheat Leaves Using UPLC-ESI-MS/MS." *Molecules* 24: 1310.

Li, Z. X., G. G. Geng, H. C. Xie, L. Y. Zhou, L. H. Wang, and F. Qiao. 2024. "Metabolomic and Transcriptomic Reveal Flavonoid Biosynthesis and Regulation Mechanism in Phlomoides Rotata From Different Habitats." *Genomics* 116: 110850.

Lin, N., X. Liu, W. Zhu, et al. 2021. "Ambient Ultraviolet B Signal Modulates Tea Flavor Characteristics via Shifting a Metabolic Flux in Flavonoid Biosynthesis." *Journal of Agricultural and Food Chemistry* 69: 3401–3414.

Liu, S., X. Y. Gu, Y. B. Jiang, et al. 2023. "UV-B Promotes Flavonoid Biosynthesis in *Ginkgo biloba* by Inducing the GbHY5-GbMYB1-GbFLS Module." *Horticulture Research* 10: uhad118.

Livak, K. J., and T. D. Schmittgen. 2001. "Analysis of Relative Gene Expression Data Using Real-Time Quantitative PCR and the 2(-Delta Delta C(T)) Method." *Methods* 25: 402–408.

Lundberg, E., and G. H. H. Borner. 2019. "Spatial Proteomics: A Powerful Discovery Tool for Cell Biology." *Nature Reviews Molecular Cell Biology* 20: 285–302.

Luo, B. B., L. J. Chen, G. P. Chen, et al. 2022. "Transcription and Metabolism Pathways of Anthocyanin in Purple Shamrock (*Oxalis triangularis* A.St.-Hil.)." *Metabolites* 12: 1290.

McInnes, K. J., J. J. J. van der Hooft, A. Sharma, et al. 2023. "Overexpression of *Brassica napus* COMT1 in Arabidopsis Heightens UV-B-Mediated Resistance to Plutella Xylostella Herbivory." *Photochemical & Photobiological Sciences* 22: 2341–2356.

Misra, P., A. Pandey, M. Tiwari, et al. 2010. "Modulation of Transcriptome and Metabolome of Tobacco by *Arabidopsis* Transcription Factor, AtMYB12, Leads to Insect Resistance." *Plant Physiology* 152: 2258–2268.

Mittler, R., S. I. Zandalinas, Y. Fichman, and F. Van Breusegem. 2022. "Reactive Oxygen Species Signalling in Plant Stress Responses." *Nature Reviews Molecular Cell Biology* 23: 663–679.

Naik, J., P. Misra, P. K. Trivedi, and A. Pandey. 2022. "Molecular Components Associated With the Regulation of Flavonoid Biosynthesis." *Plant Science* 317: 111196.

Nishimoto, Y., O. Ohnishi, and M. Hasegawa. 2003. "Topological Incongruence Between Nuclear and Chloroplast DNA Trees Suggesting Hybridization in the Urophyllum Group of the Genus (Polygonaceae)." *Genes & Genetic Systems* 78: 139–153.

Ohsako, T., and C. Y. Li. 2020. "Classification and Systematics of the Species." *Breeding Science* 70: 93–100.

Ohsako, T., K. Yamane, and O. Ohnishi. 2002. "Two New Fagopyrum (Polygonaceae) Species, *F. gracilipedoides* and *F. jinshaense* From Yunnan, China." *Genes & Genetic Systems* 77: 399–408.

Olarte, R. A., J. Menke, Y. Zhang, et al. 2019. "Chromosome Rearrangements Shape the Diversification of Secondary Metabolism in the Cyclosporin Producing Fungus." *BMC Genomics* 20: 120.

Peng Dechuan, T. Y., J. Sun, and J. Liu. 2006. "Determination and Comparison of Flavonoid Content in Tartary Buckwheat and Several Wild Buckwheat Species." *Proceedings of the International Forum on Tartary Buckwheat Industry Economics. Chinese* 2: 4.

Peng, M., R. Shahzad, A. Gul, et al. 2017. *Differentially Evolved Glucosyltransferases Determine Natural Variation of Rice Flavone Accumulation and UV-Tolerance*. Nature communications 8: 1975.

Podolec, R., and R. Ulm. 2018. "Photoreceptor-Mediated Regulation of the COP1/SPA E3 Ubiquitin Ligase." *Current Opinion in Plant Biology* 45: 18–25.

Raskina, O., J. C. Barber, E. Nevo, and A. Belyayev. 2008. "Repetitive DNA and Chromosomal Rearrangements: Speciation-Related Events in Plant Genomes." *Cytogenetic and Genome Research* 120: 351–357.

Ryan, K. G., E. E. Swinny, K. R. Markham, and C. Winefield. 2002. "Flavonoid Gene Expression and UV Photoprotection in Transgenic and Mutant Leaves." *Phytochemistry* 59: 23–32.

Saxena, S., G. Pal, and A. Pandey. 2023. "Functional Characterization of 2-Oxoglutarate-Dependent Dioxygenase Gene Family in Chickpea." *Plant Science* 336: 111836.

Schenk, J. J., L. E. Becklund, S. J. Carey, and P. P. Fabre. 2023. "What Is the "Modified" CTAB Protocol? Characterizing Modifications to the

CTAB DNA Extraction Protocol." *Applications in Plant Sciences* 11: e11517.

Shi, C., and H. T. Liu. 2021. "How Plants Protect Themselves From Ultraviolet-B Radiation Stress." *Plant Physiology* 187: 1096–1103.

Sleator, R. D. 2016. "JCVI-syn3.0-A Synthetic Genome Stripped Bare!" *Bioengineered* 7: 53–56.

Solovchenko, A., and M. Schmitz-Eiberger. 2003. "Significance of Skin Flavonoids for UV-B-Protection in Apple Fruits." *Journal of Experimental Botany* 54: 1977–1984.

Takahashi, M., M. Teranishi, H. Ishida, et al. 2011. "Cyclobutane Pyrimidine Dimer (CPD) Photolyase Repairs Ultraviolet-B-Induced CPDs in Rice Chloroplast and Mitochondrial DNA." *Plant Journal* 66: 433–442.

Tian, X., M. X. Hu, J. Yang, Y. Q. Yin, and W. M. Fang. 2024. "Ultraviolet-B Radiation Stimulates Flavonoid Biosynthesis and Antioxidant Systems in Buckwheat Sprouts." *Food* 13: 3650.

Vogt, T., and P. Jones. 2000. "Glycosyltransferases in Plant Natural Product Synthesis: Characterization of a Supergene Family." *Trends in Plant Science* 5: 380–386.

Wang, L. F., G. H. Jia, X. Y. Jiang, S. Cao, Z. J. Chen, and Q. X. Song. 2021. "Altered Chromatin Architecture and Gene Expression During Polyploidization and Domestication of Soybean." *Plant Cell* 33: 1430–1446.

Wang, M., Y. Zhang, C. Y. Zhu, et al. 2021. "Overexpression Promotes Flavonoid Accumulation and Abiotic Stress Tolerance in Plant." *Physiologia Plantarum* 172: 1966–1982.

Wang, M. Y., Q. S. Ji, B. Lai, Y. R. Liu, and K. R. Mei. 2023. "Structure-Function and Engineering of Plant UDP-Glycosyltransferase." *Computational and Structural Biotechnology Journal* 21: 5358–5371.

Waterhouse, A., M. Bertoni, S. Bienert, et al. 2018. "SWISS-MODEL: Homology Modelling of Protein Structures and Complexes." *Nucleic Acids Research* 46: W296–W303.

Wen, W., Z. Q. Li, J. R. Shao, et al. 2021. "The Distribution and Sustainable Utilization of Buckwheat Resources Under Climate Change in China." *Plants* 10: 2081.

Wolfe, K., and C. O'hUigín. 2016. "Significance of Positive Selection and Gene Duplication in Adaptive Evolution: In Memory of Austin L. Hughes." *Immunogenetics* 68: 749–753.

Wu, H. M., D. J. Xie, P. F. Jia, et al. 2023. "Homeostasis of Flavonoids and Triterpenoids Most Likely Modulates Starch Metabolism for Pollen Tube Penetration in Rice." *Plant Biotechnology Journal* 21: 1757–1772.

Xie, L. F., Y. Guo, C. H. Ren, et al. 2022. "Unravelling the Consecutive Glycosylation and Methylation of Flavonols in Peach in Response to UV-B Irradiation." *Plant, Cell and Environment* 45: 2158–2175.

Xue, C. X., F. T. Qiu, Y. X. Wang, et al. 2023. "Tuning Plant Phenotypes by Precise, Graded Downregulation of Gene Expression." *Nature Biotechnology* 41: 1758–1764.

Yan, D. W., L. Duermeyer, C. Leoveanu, and E. Nambara. 2014. "The Functions of the Endosperm During Seed Germination." *Plant & Cell Physiology* 55: 1521–1533.

Yang, A., K. M. Jude, B. Lai, et al. 2023. "Deploying Synthetic Coevolution and Machine Learning to Engineer Protein-Protein Interactions." *Science* 381: 412.

Yang, F., L. Zhang, X. Zhang, et al. 2024. "Genome-Wide Investigation of UDP-Glycosyltransferase Family in Tartary Buckwheat (*Fagopyrum tataricum*)." *BMC Plant Biology* 24: 249.

Yasui, Y., and O. Ohnishi. 1998. "Interspecific Relationships in Fagopyrum (Polygonaceae) Revealed by the Nucleotide Sequences of the rbcL and accD Genes and Their Intergenic Region." *American Journal of Botany* 85: 1134–1142.

Yu, X. F., Y. L. Zhu, J. Y. Fan, D. J. Wang, X. H. Gong, and Z. Ouyang. 2017. "Accumulation of Flavonoid Glycosides and UFGT Gene Expression in *Mulberry Leaves* (L.) Before and After Frost." *Chemistry & Biodiversity* 14: e1600496.

Zargar, S. M., A. Hami, M. Manzoor, et al. 2024. "Buckwheat OMICS: Present Status and Future Prospects." *Critical Reviews in Biotechnology* 44: 717–734.

Zeng, X. Q., H. J. Yuan, X. K. Dong, et al. 2020. "Genome-Wide Dissection of co-Selected UV-B Responsive Pathways in the UV-B Adaptation of Qingke." *Molecular Plant* 13: 112–127.

Zhang, F., H. Guo, J. C. Huang, et al. 2020. "A UV-B-Responsive Glycosyltransferase, OsUGT706C2, Modulates Flavonoid Metabolism in Rice." *Science China. Life Sciences* 63: 1037–1052.

Zhang, F., J. C. Huang, H. Guo, et al. 2022. "Contributes to Flavonoid Accumulation and UV-B Tolerance by Regulating in Rice." *Science China. Life Sciences* 65: 1380–1394.

Zhang, J., Y. Tian, L. Yan, et al. 2016. "Genome of Plant Maca (*Lepidium meyenii*) Illuminates Genomic Basis for High-Altitude Adaptation in the Central Andes." *Molecular Plant* 9: 1066–1077.

Zhang, K. X., M. He, Y. Fan, et al. 2021. "Resequencing of Global Tartary Buckwheat Accessions Reveals Multiple Domestication Events and Key Loci Associated With Agronomic Traits." *Genome Biology* 22: 23.

Zhang, K. X., Y. Q. He, X. Lu, et al. 2023. "Comparative and Population Genomics of Buckwheat Species Reveal Key Determinants of Flavor and Fertility." *Molecular Plant* 16: 1427–1444.

Zhang, L. J., X. X. Li, B. Ma, et al. 2017. "The Tartary Buckwheat Genome Provides Insights Into Rutin Biosynthesis and Abiotic Stress Tolerance." *Molecular Plant* 10: 1224–1237.

Zhao, H., Y. He, K. Zhang, et al. 2023. "Rewiring of the Seed Metabolome During Tartary Buckwheat Domestication." *Plant Biotechnology Journal* 21: 150–164.

Zhao, H. X., M. F. Hu, Y. Fang, et al. 2024. "Regulatory Module FtMYB5/6-FtGBF1-Promotes Rutin Biosynthesis in Tartary Buckwheat." *Journal of Agricultural and Food Chemistry* 72: 12630–12640.

Zhong, L. Y., Y. J. Lin, C. Wang, et al. 2022. "Chemical Profile, Antimicrobial and Antioxidant Activity Assessment of the Crude Extract and Its Main Flavonoids From Tartary Buckwheat Sprouts." *Molecules* 27: 374.

Zhou, B. T., P. Hu, G. C. Liu, et al. 2024. "Evolutionary Patterns and Functional Effects of 3D Chromatin Structures in Butterflies With Extensive Genome Rearrangements." *Nature Communications* 15: 6303.

Supporting Information

Additional supporting information can be found online in the Supporting Information section. **Figure S1:** Measurement of metabolite content in seeds of different buckwheat varieties. **Figure S2:** Growth status of *F. urophyllum*, *F. gracilipes*, *F. tataricum*, *F. cymosum* and *F. esculentum* seedlings. **Figure S3:** Rutin-related metabolite content of Tartary buckwheat accessions at different altitudes. **Figure S4:** Effects of rutin-related metabolites treatment on UV-B phenotypes of plants. **Figure S5:** Chromosomal mapping of *FLS*, *UF3GT* and *RT* in different buckwheat varieties. **Figure S6:** Chromosomal synteny of *FLS*, *UF3GT* and *RT*. **Figure S7:** Analysis of the *FLS* gene family and selection pressure in buckwheat. **Figure S8:** Functional analysis of the *FtFLS4* G125D mutation. **Figure S9:** Analysis of UV-B treatment effects on *FLS* promoter activity. **Figure S10:** Weighted gene co-expression network analysis. **Figure S11:** UV-B response of the *UF3GT* promoter. **Figure S12:** Effects of the T255P mutation in *FtUF3GT1* and *FgUF3GT19* on enzyme function. **Figure S13:** Analysis of the *UF3GT* gene family and selection pressure in buckwheat. **Figure S14:** Substrate analysis of *FtRT1*. **Figure S15:** Analysis of *RT* gene copy numbers and expression levels in buckwheat. **Figure S16:** Catalytic conditions analysis. **Figure S17:** Kinetic constants of *FtRT1* and *FgRT1*. **Figure S18:** Rutin and

nicotiflorin content in *FgRT1*-OE hairy root. **Figure S19:** Prediction and validation of the catalytic centre of *FtRT1*. **Figure S20:** Cellular characteristics of key site mutations in *FtRT1* and their effects on metabolite synthesis in overexpressed hairy roots. **Figure S21:** Visualisation of differential amino acids near key amino acid sites of *FtRT1* and *FgRT1*. **Figure S22:** Promoter activity analysis of *RT* under UV-B treatment. **Figure S23:** Flavonoid content and DAB, NBT staining in overexpressing *Arabidopsis*. **Figure S24:** Identification of overexpressed hairy roots and *Arabidopsis*. **Table S1:** Metabolite content of different varieties of buckwheat. **Table S2:** Analysis of physicochemical properties of *FLS*, *UF3GT* and *RT* genes in buckwheat. **Table S3:** Candidate genes associated with leading SNP Ft: 8330589 on Chr5 for quercetin-7-O-(6′-O-malonyl)-β-D-glucoside content GWAS. **Table S4:** Correlation analysis of FtRT1 and FtUF3GT1 with hub genes in WGCNA networks. **Table S5:** Statistics on the number of different promoter elements. **Table S6:** Primers used in this study.